

Effects of Antenna Height and Directivity on 60 GHz Indoor Channels

Jie Huang¹, Yu Liu¹, Jian Sun^{1,2}, Wensheng Zhang¹, and Cheng-Xiang Wang³

¹Shandong Provincial Key Lab of Wireless Communication Technologies, Shandong University, Jinan, 250100, China.

²State Key Lab. of Millimeter Waves, Southeast University, Nanjing, 210096, China.

³Institute of Sensors, Signals and Systems, School of Engineering & Physical Sciences, Heriot-Watt University, Edinburgh, EH14 4AS, UK.

Email: hj_1204@sina.cn, xinwenliyu@163.com, sunjian@sdu.edu.cn, zhangwsh@sdu.edu.cn, cheng-xiang.wang@hw.ac.uk

Abstract—Millimeter wave (mmWave) communication is a key technology for the fifth generation (5G) wireless communications, especially the 60 GHz bands for short-range indoor communications. Though there have been many channel measurements at 60 GHz bands, few of them concern about antenna effects on the propagation channel characteristics, such as the antenna height and directivity effects. In this paper, we conduct extensive 60 GHz indoor channel measurements. Different antenna height and directivity configurations are utilized, and the effects on the propagation channel characteristics are investigated, especially the average power delay profile (APDP), K-factor, root mean square (RMS) delay spread (DS), and RMS angle spread (AS). The results will be valuable for the design of 5G mmWave communication systems.

Index Terms—Millimeter wave, 60 GHz, 5G, channel measurements, antenna effects.

I. INTRODUCTION

MmWave communication is a key technology for the 5G wireless communications [1], especially for short-range indoor scenarios. There are at least 5 GHz unlicensed bandwidths around 60 GHz almost all over the world. MmWave benefits from huge bandwidths and can be utilized to achieve high data rate, low latency, and high energy efficiency and cost efficiency. Several standards have been developed at 60 GHz bands such as IEEE 802.15.3c for wireless personal area network (WPAN) [2], IEEE 802.11ad for wireless local area network (WLAN) [3], and IEEE 802.11ay for next generation wireless fidelity (WiFi) [4]. One of the main problems is the additional path loss compared to the sub-6 GHz frequency bands. The high path loss can be mitigated by beamforming with high gain antennas.

Various channel measurements have been conducted at 60 GHz bands in many typical indoor scenarios, such as the office, corridor, hall, and so on [5]–[8], in order to study the propagation channel characteristics. However, few of them concerned about the antenna effects. Most of the 60 GHz channel measurements were conducted with specific type of antennas, which were located with given heights. An early work [9] investigated the effects of antenna directivity on 60 GHz indoor communication. An image based ray tracing model was used to analyze the variations of the received power, RMS DS, and K-factor. In [10], the authors conducted 60 GHz indoor channel measurements and investigated the impact of antenna pattern on large-scale path loss.

Actually, the response of the antenna pattern is usually embedded in the measured channel impulse response (CIR).

For 60 GHz indoor channel measurements, high gain horn antennas are usually applied to achieve a high system dynamic range. The directivity of the antenna will impact the power of multipath components (MPCs). A high directive horn antenna can provide high gains in a narrow beamwidth, while an omnidirectional antenna can provide coverage almost over the whole space. If the transmitter (Tx) and receiver (Rx) antennas are at the same height, a two dimensional (2D) distance and only azimuth angle are enough to describe the channel. If the antennas are at different heights, a three dimensional (3D) distance and elevation angle may be needed.

To investigate the antenna effects, we carry out extensive 60 GHz channel measurements in a typical indoor office environment. Different antenna heights and patterns are utilized. To estimate the angle information, uniform virtual array measurement method [11] is used. The high resolution space alternating generalized expectation-maximization (SAGE) algorithm [12] is then applied to process the measurement data to study the antenna effects.

The remainder of this paper is organized as follows. Section II describes the measurement environment and measurement system setup. In Section III, the post-processing methods are presented. Antenna effects on the 60 GHz propagation channel characteristics are analyzed in Section IV. Finally, conclusions are drawn in Section V.

II. MMWAVE CHANNEL MEASUREMENTS

A. Measurement Environment

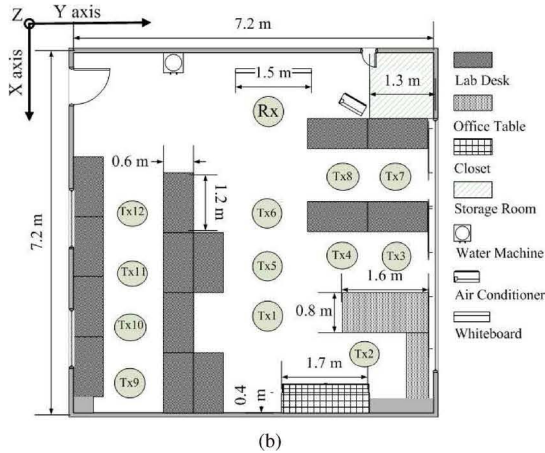
The channel measurements are conducted in an indoor office environment with room size of $7.2 \times 7.2 \times 3 \text{ m}^3$, as shown in Fig. 1(a). The layout and sizes of main objects in the office are shown in Fig. 1(b). The walls, floor, and ceiling are made of concrete. Parts of the floor and ceiling are made of anti-static-electricity board. There are several windows on both sides of the wall. More detailed descriptions about the environment can be found in [11].

B. Measurement System Setup

Indoor channel measurements are usually conducted in frequency domain with a vector network analyzer (VNA). However, the measurable distance is limited due to the cable connection. To deal with the shortage, an additional signal generator is used. The channel sounder mainly consists of a



(a)



(b)

Fig. 1. (a) photo of the environment and (b) layout of the environment.

Keysight E8257D signal generator and a Keysight N5227A VNA, as shown in Fig. 2. The transmit power is 13 dBm, the sweeping frequencies are from 59 GHz to 61 GHz with 401 points, and the intermediate filter (IF) bandwidth is set as 1 kHz. The Tx antenna is a Flann MD249-AA omni-directional antenna [13] which is supported by a high-accuracy antenna positioner to shift positions in X/Y/Z axes. The Tx antenna scans in a $15 \times 15 \times 6$ hollow cube array which is formed of six surfaces of a cube array. The spacing step of the antenna array is set as 2.5 mm, which is half a wavelength at 60 GHz. A total of twelve Tx locations are selected, as shown in Fig. 1(b). The height of Tx antenna array is set as either 1.6 m or 2 m. The Rx antenna is an Ainfo standard gain horn antenna [14] which is supported by a tripod at the height of 1.6 m and aligned to X axis. The horn antenna is either a high gain narrow half power beamwidth (HPBW) antenna or a low gain wide HPBW antenna. For the 25 dBi horn antenna, the HPBW is 10° , while it is 55° for the 10 dBi horn antenna. Photos of the omni-directional antenna and horn antennas are shown in Fig. 3. The measurements are automatically controlled by a laptop with the environment being kept quasi-static. Once the Tx antenna moves to a predefined position in the array, the signal generator is triggered and swept in the defined frequency bands, and the fading signal is received by the VNA. A back-to-back calibration is conducted before the measurement so as to remove the responses of the measurement system and cables.

In order to investigate the antenna effects on propagation

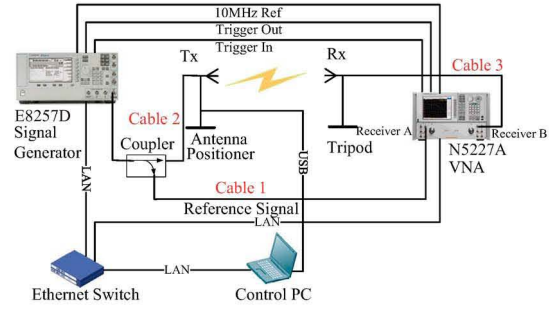


Fig. 2. Measurement system setup.

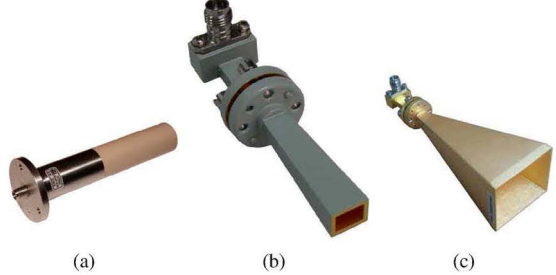


Fig. 3. Photos of (a) omni-directional antenna, (b) 10 dBi horn antenna, and (c) 25 dBi horn antenna.

TABLE I
DIFFERENT ANTENNA CONFIGURATIONS FOR 60 GHZ CHANNEL MEASUREMENTS.

Configuration	Tx height (m)	Rx gain (dBi)	Rx HPBW ($^\circ$)
C1	1.6	25	10
C2	2	25	10
C3	1.6	10	55
C4	2	10	55

tion channel characteristics, different antenna configurations should be applied. Due to the time consuming of channel measurements, only four channel measurement campaigns are conducted with different antenna configurations, including the antenna height and gain configurations, as shown in Table I. The measurement data with different antenna configurations is then processed to analyze the antenna effects.

III. MEASUREMENT DATA PROCESSING METHODS

The measured channel transfer function (CTF) at each Tx location is a $N \times K$ matrix $H(n, k), n = 1, \dots, N; k = 1, \dots, K$, where $N = 15 \times 15 \times 6$ is the array size, and $K = 401$ is the sweeping frequency points. The CIR $h(n, k) \in \mathbb{C}^{N \times K}$ can be obtained from the measured CTF via inverse Fourier transform. The power delay profile (PDP) is obtained as $|h(n, k)|^2$. The APDP is then obtained by averaging the PDPs over the Rx hollow cube array,

$$APDP(dB) = 10\log_{10}\left(\frac{1}{N} \sum_{n=1}^N |h(n, k)|^2\right), k = 1, \dots, K. \quad (1)$$

The K-factor which is the power ratio between line-of-sight (LOS) component and nonline-of-sight (NLOS) components can also be obtained.

For VNA-based channel measurements, due to the quasi-static nature of the environment and relatively long measurement time, only a single snapshot of the channel is measured. The maximum likelihood (ML) based SAGE algorithm is then applied to the data post-processing to extract MPC parameters.

In the SAGE algorithm, the number of MPCs L is usually predefined large enough to capture all the significant paths. A good trade-off between accuracy and computational complexity can be achieved when the number of MPCs equals 100. The outputs of the SAGE algorithm are the parameter sets $\Theta_l = [\alpha_l, \tau_l, \phi_l, \theta_l], l = 1, \dots, L$, where α_l , τ_l , ϕ_l , and θ_l denote the complex amplitude, delay, azimuth angle, and elevation angle of the l th MPC, respectively. More details about the implementation of the SAGE algorithm and the post-processing methods can be found in [15].

The RMS DS can be calculated as

$$DS = \sqrt{\frac{\sum_1^L |\alpha_l|^2 \tau_l^2}{\sum_1^L |\alpha_l|^2} - \left(\frac{\sum_1^L |\alpha_l|^2 \tau_l}{\sum_1^L |\alpha_l|^2}\right)^2}. \quad (2)$$

The RMS AS is calculated as

$$AS = \sqrt{\frac{\sum_1^L |\alpha_l|^2 \psi_l^2}{\sum_1^L |\alpha_l|^2} - \left(\frac{\sum_1^L |\alpha_l|^2 \psi_l}{\sum_1^L |\alpha_l|^2}\right)^2} \quad (3)$$

where ψ_l denotes the azimuth angle ϕ_l or elevation angle θ_l .

IV. RESULTS AND ANALYSIS

As an example, the power-angle-delay-profiles (PADPs) for measurements C1 and C3 at Tx3 are shown in Fig. 4. Because different antennas are used, the PADPs show great differences, which indicates that antenna configurations will have effects on the propagation channel characteristics.

In this section, antenna effects on the APDP, K-factor, RMS DS, and RMS AS will be analyzed.

A. APDP

APDPs with different antenna configurations at the twelve Tx locations are obtained from the measurement data. For measurements C1 and C2, as the Rx antenna is a high gain horn antenna, its coverage range is mainly concentrated on the main lobe direction. Thus, Tx1, Tx2, Tx5, Tx6, Tx9, and Tx10 are LOS scenarios, while the others are NLOS scenarios. For C3 and C4, as the HPBW of the horn antenna is 55° , it can coverage a wide range. Thus, only Tx7 is NLOS scenario, while other Tx locations are LOS scenarios. As an example, APDPs with different antenna configurations at Tx3, Tx5, Tx7, and Tx12 are shown in Fig. 5.

Seen from Fig. 5(a), as Tx3 is out of the coverage range of a 25 dBi horn antenna, the power of LOS path is lower than reflected paths, and it is also much lower than the LOS power received by a 10 dBi horn antenna. The power of the first-order reflected path is also larger for a 10 dBi horn antenna than that of a 25 dBi horn antenna.

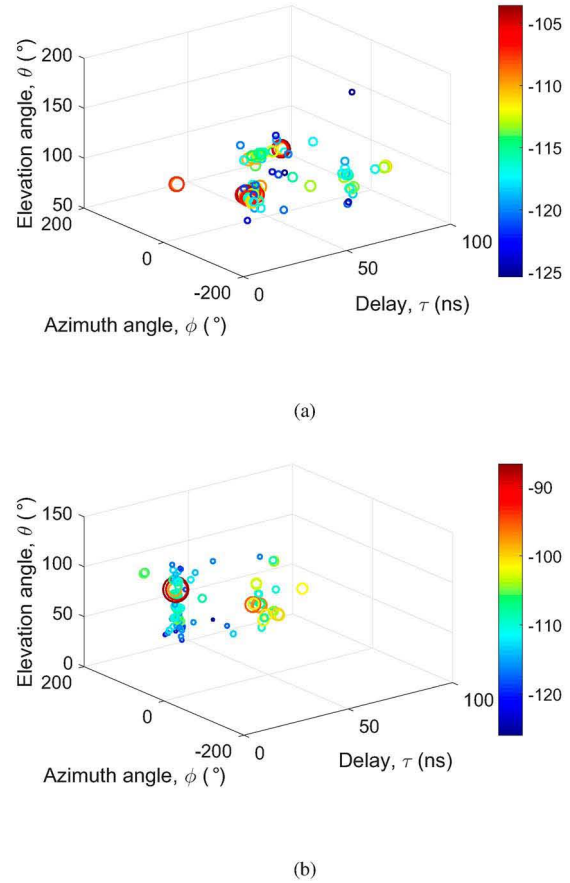


Fig. 4. PADPs at Tx3 for (a) measurement C1 and (b) measurement C3.

For strong LOS scenarios, such as Tx5 shown in Fig. 5(b), by comparing C1 and C2 with C3 and C4, we can see that a higher antenna gain can achieve larger powers for both the LOS path and reflected paths.

As Tx7 is out of the coverage range of the 10 dBi horn antenna, it is NLOS scenario, as shown in Fig. 5(c). Though the LOS received power is larger for a 10 dBi horn antenna, the reflected paths show smaller powers for a 10 dBi horn antenna than that of a 25 dBi horn antenna.

For Tx12 shown in Fig. 5(d), it is NLOS scenario when using 25 dBi horn antenna, but it is LOS scenario for 10 dBi horn antenna. For reflected path with delay about 36 ns, the received power is at the same level for different Rx antennas, while the powers of multiple reflected paths are larger for 25 dBi horn antenna.

From Fig. 5, we can also see that antennas at the same height can relatively receive more powers for 25 dBi horn antenna, but the difference can almost be ignored for 10 dBi horn antenna.

B. K-factor

The antenna configuration also has effect on K-factor. Table II shows the calculated K-factor for different antenna configurations at the twelve Tx locations. For measurement C1, the K-factor ranges between -29.7 dB and 19.9 dB, while

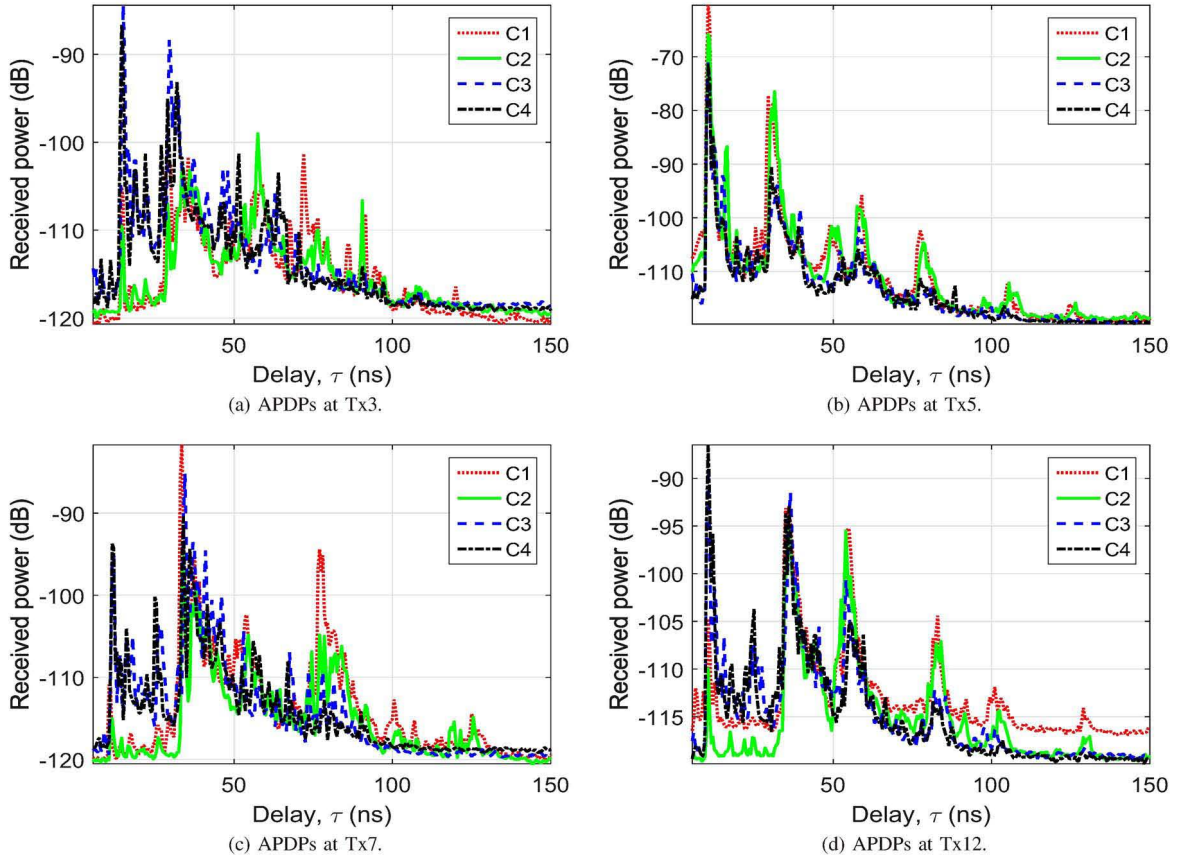


Fig. 5. APDPs with different antenna configurations at (a) Tx3, (b) Tx5, (c) Tx7, and (d) Tx12.

it is in a smaller range from -22.7 dB to 13.0 dB for C2. Tx1, Tx5, and Tx6 are strong LOS scenarios, Tx2, Tx9, and Tx10 are weak LOS scenarios, and Tx7 and Tx8 can be classified as strong NLOS scenarios. In general, measurements C1 and C2 have comparable K-factors at the same Tx locations, which means that the antenna height difference of 0.4 m has a relatively small effect on K-factor, except the strong LOS and strong NLOS scenarios.

For measurements using 10 dBi horn antenna, the K-factor varies in a relatively small range at the twelve Tx locations, except the strong LOS scenarios at Tx1, Tx5, and Tx6 locations. The K-factor also has comparable values for C3 and C4 at the same Tx locations.

Comparing C1 with C3 and C2 with C4, we can see that the situations of Tx3, Tx4, Tx8, Tx11, and Tx12 change from LOS scenario to NLOS scenario, which verifies that the 10 dBi horn antenna has a better coverage range than that of the 25 dBi horn antenna.

C. RMS DS

The RMS DS for different antenna configurations is shown in Table III. Generally speaking, NLOS scenarios have larger RMS DS than that of LOS scenarios. As seen from Table III, for strong LOS scenarios, the RMS DS is within 5 ns, which is very

TABLE II
K-FACTOR FOR DIFFERENT ANTENNA CONFIGURATIONS.

K-factor (dB)	C1	C2	C3	C4
Tx1	12.0	13.0	8.6	11.5
Tx2	-2.1	-2.2	3.8	2.4
Tx3	-8.8	-13.8	2.7	3.5
Tx4	-9.4	-8.5	8.8	11.1
Tx5	14.3	10.2	18.1	18.3
Tx6	19.9	9.3	18.5	14.9
Tx7	-29.7	-22.7	-10.9	-5.5
Tx8	-26.9	-22.0	3.8	3.1
Tx9	2.2	-1.6	8.8	6.0
Tx10	-5.0	-5.3	4.4	8.5
Tx11	-14.6	-9.6	8.4	9.1
Tx12	-14.0	-18.1	1.4	5.5

low compared with NLOS scenarios. In general, Tx antenna at 2 m height has a little larger RMS DS compared with height of 1.6 m. For Tx1, Tx5, and Tx6 locations which are always strong LOS scenarios, the 25 dBi horn antenna can achieve smaller RMS DS values. However, it is contrary to the other Tx locations. As most of the other Tx locations change from NLOS to LOS scenarios when a 10 dBi horn antenna is used instead, the RMS DS values are smaller for 10 dBi horn antenna. Also, by comparing the K-factor shown in Table II with the RMS

TABLE III
RMS DS FOR DIFFERENT ANTENNA CONFIGURATIONS.

RMS DS (ns)	C1	C2	C3	C4
Tx1	2.5	3.4	4.6	4.8
Tx2	18.1	20.7	3.7	2.4
Tx3	19.9	14.1	7.7	8.9
Tx4	17.7	15.9	5.5	3.9
Tx5	1.7	5.1	1.5	2.7
Tx6	0.24	7.5	1.3	2.5
Tx7	10.8	14.2	7.4	10.7
Tx8	7.4	8.7	11.2	14.7
Tx9	16.2	17.4	4.4	3.9
Tx10	14.2	17.0	6.2	5.2
Tx11	15.1	12.2	8.4	9.0
Tx12	10.8	9.4	13.4	12.4

TABLE IV
RMS AAS AND EAS FOR DIFFERENT ANTENNA CONFIGURATIONS.

RMS AAS /EAS($^{\circ}$)	C1	C2	C3	C4
Tx1	60.8/7.0	57.1/8.9	68.1/12.7	71.7/11.1
Tx2	72.0/5.5	71.4/5.8	56.2/11.0	104.7/11.5
Tx3	61.8/4.6	61.6/4.8	60.2/9.2	58.7/7.2
Tx4	71.8/5.9	73.7/5.2	39.3/9.9	30.0/10.5
Tx5	58.8/13.2	53.8/9.1	60.5/11.6	46.2/7.3
Tx6	43.1/9.3	60.2/10.3	48.6/11.2	42.5/7.8
Tx7	48.7/6.8	58.1/5.3	57.2/5.4	58.7/8.4
Tx8	75.5/7.4	70.5/7.1	53.6/8.1	43.0/8.3
Tx9	112.8/7.6	110.0/5.3	84.6/7.1	100.3/6.2
Tx10	107.1/4.7	104.7/5.2	96.9/6.5	79.4/8.7
Tx11	68.1/4.9	36.6/6.0	83.3/8.9	70.6/7.0
Tx12	93.1/4.3	78.5/6.2	99.4/9.2	105.0/8.6

DS shown in Table III, a strong negative correlation can be found between K-factor and RMS DS. That is to say, when the K-factor is high, the RMS DS is small, and it becomes large when the K-factor is low.

D. RMS AS

The calculated RMS azimuth AS (AAS) and elevation AS (EAS) are shown in Table IV. Comparing C1 with C2 and C3 with C4, similar RMS AAS and EAS values can be found at most Tx locations when using the same Rx antenna, which means that the antenna height difference of 0.4 m has marginal effect on the RMS AAS and EAS.

The RMS AAS varies in a wide range between 30° and 113° for all the measurements. However, values of the RMS EAS are within 10° for most of the measurements. Meanwhile, no direct influence of the antenna directivity on RMS AS is found. The reason may be that the RMS AS is mainly influenced by the measurement environment. Due to multiple reflections, MPCs will arrive with angles distributed in the space. Different antenna patterns can achieve different RMS AS values.

V. CONCLUSIONS

In this paper, we have conducted extensive channel measurements at 60 GHz frequency bands in an indoor office environment. Different antenna configurations including the

antenna height and directivity have been utilized. The measurement data has been processed with the SAGE algorithm, and antenna effects on propagation channel characteristics have been investigated, especially the effects on the APDP, K-factor, RMS DS, and RMS AS. The results will be valuable for the design of 5G mmWave communication systems.

ACKNOWLEDGMENT

The authors would like to acknowledge the support from the Natural Science Foundation of China (Grant No. 61371110, 61771293), Fundamental Research Funds of Shandong University (No. 2017JC029), EU H2020 RISE TESTBED project (Grant No. 734325), EU FP7 QUICK project (Grant No. PIRSES-GA-2013-612652), and EPSRC TOUCAN project (Grant No. EP/L020009/1).

REFERENCES

- [1] C.-X. Wang, F. Haider, X. Gao, X.-H. You, Y. Yang, D. Yuan, H. Aggoune, H. Haas, S. Fletcher, and E. Hepsaydir, "Cellular architecture and key technologies for 5G wireless communication networks," *IEEE Commun. Mag.*, vol. 52, no. 2, pp. 122–130, Feb. 2014.
- [2] S.-K. Yong, *TG3c Channel Modeling Sub-Committee Final Report*, IEEE Standard 802.15-07-0584-01-003c, Mar. 2007.
- [3] A. Maltsev *et al.*, *Channel Models for 60 GHz WLAN Systems*, IEEE Standard 802.11-09/0334r8, May 2010.
- [4] A. Maltsev *et al.*, *Channel Models for IEEE 802.11ay*, IEEE Standard 802.11-15/11509r, May 2016.
- [5] N. Moraitsis and P. Constantinou, "Measurements and characterization of wideband indoor radio channel at 60 GHz," *IEEE Trans. Wireless Commun.*, vol. 5, no. 4, pp. 880–889, Apr. 2006.
- [6] S. Geng, J. Kivinen, X. Zhao, and P. Vainikainen, "Millimeter-wave propagation channel characterization for short-range wireless communications," *IEEE Trans. Veh. Technol.*, vol. 58, no. 1, pp. 3–13, Jan. 2009.
- [7] M. Kyro, J. Simola, K. Haneda, S. Ranvier, P. Vainikainen, and K. Takizawa, "60 GHz radio channel measurements and modeling in a shielded room," in *Proc. IEEE VTC'10-Spring*, Taipei, China, May 2010, pp. 1–5.
- [8] C. Gustafson, K. Haneda, S. Wyne, and F. Tufvesson, "On mm-wave multipath clustering and channel modeling," *IEEE Trans. Antennas Propag.*, vol. 62, no. 3, pp. 1445–1455, Mar. 2014.
- [9] M. R. Williamson, G. E. Athanasiadou, and A. R. Nix, "Investigating the effects of antenna directivity on wireless indoor communication at 60 GHz," in *Proc. IEEE PIMRC'97*, Helsinki, Finland, Sept. 1997, pp. 635–639.
- [10] H. Yang, M. Herben, and P. F. M. Smulders, "Impact of antenna pattern and reflective environment on 60 GHz indoor radio channel characteristics," *IEEE Antennas Wireless Propag. Lett.*, vol. 4, pp. 300–303, 2005.
- [11] X. Wu, C.-X. Wang, J. Sun, J. Huang, R. Feng, Y. Yang, and X. Ge, "60 GHz millimeter-wave channel measurements and modeling for indoor office environments," *IEEE Trans. Antennas Propag.*, vol. 65, no. 4, pp. 1912–1924, Apr. 2017.
- [12] B. H. Fleury, M. Tschudin, R. Heddergott, D. Dahlhaus, and K. I. Pedersen, "Channel parameter estimation in mobile radio environments using the SAGE algorithm," *IEEE J. Sel. Areas Commun.*, vol. 17, no. 3, pp. 434–450, Mar. 1999.
- [13] Flann company, [Online]. Available: <http://flann.com/wp-content/uploads/2015/09/Series-MD249.pdf>
- [14] Ainfo company, [Online]. Available: http://www.ainfoinc.cn/cn/p_ant_h_std.asp
- [15] J. Huang, C.-X. Wang, R. Feng, J. Sun, W. Zhang, and Y. Yang, "Multi-frequency mmWave massive MIMO channel measurements and characterization for 5G wireless communication systems," *IEEE J. Sel. Areas Commun.*, vol. 35, no. 7, pp. 1591–1605, Jul. 2017.